Artificial Intelligence Aided Automated Design for Reliability of Power Electronic Systems

Dragicevic, Tomislav; Wheeler, Patrick; Blaabjerg, Frede

Published in:
I E E E Transactions on Power Electronics

DOI (link to publication from Publisher):
10.1109/TPEL.2018.2883947

Publication date:
2019

Document Version
Accepted author manuscript, peer reviewed version

Artificial Intelligence Aided Automated Design for Reliability of Power Electronic Systems

Tomislav Dragičević, *Senior Member, IEEE*, Patrick Wheeler, *Senior Member, IEEE*, and Frede Blaabjerg, *Fellow, IEEE*

***Abstract*—This paper proposes a new methodology for automated design of power electronic systems realized through the use of artificial intelligence. Existing approaches do not consider the system's reliability as a performance metric or are limited to reliability evaluation for a certain fixed set of design parameters. The method proposed in this paper establishes a functional relationships between design parameters and reliability metrics, and uses them as the basis for optimal design. The first step in this new framework is to create a nonparametric surrogate model of the power converter that can quickly map the variables characterizing the operating conditions (e.g. ambient temperature, irradiation) and design parameters (e.g. switching frequency, dc link voltage) into variables characterizing the thermal stress of a converter (e.g. mean temperature and temperature variation of its devices). This step can be carried out by training a dedicated artificial neural network (ANN) either on experimental or simulation data. The resulting network is named as ANN_1 and can be deployed as an accurate surrogate converter model. This model can then be used to quickly map the yearly mission profile into a thermal stress profile of any selected device for a large set of design parameter values. The resulting data is then used to train ANN_2, which becomes an overall system representation that explicitly maps the design parameters into a yearly lifetime consumption. To verify the proposed methodology, ANN_2 is deployed in conjunction with the standard converter design tools on an exemplary grid-connected PV converter case study. This study showed how to find the optimal balance between the reliability and output filter size in the system with respect to several design constraints. This paper is also accompanied by a comprehensive data set that was used for training the ANNs.**

***Index Terms*—Automated design for reliability (ADfR), artificial intelligence, power electronic systems.**

I. Introduction

THE use of power electronic converters has become omnipresent nowadays. They are the key enablers of technologies such as renewable energy systems, electrical vehicles and their charging infrastructure, variable speed drives, as well as uninterruptible power supply (UPS) systems and microgrids [1], [2]. Much like any other system, power converters are prone to failures. Such failures cause downtimes that often require costly maintenance procedures, especially if the power electronic system is located in the remote or offshore location. Moreover, such failures may also have catastrophic consequences in mission critical applications or significantly reduce the energy yield of renewable energy systems [3], [4].

T. Dragičević and F. Blaabjerg are with Department of Energy Technology, Aalborg University, Pontoppidanstraede 111, 9220 Aalborg East, Denmark (e-mail: tdr@aau.dk, fbl@et.aau.dk). P. Wheeler is with the Power Electronics, Machines and Control Group, The University of Nottingham, Nottingham NG7 2RD, U.K. (e-mail: pat.wheeler@nottingham.ac.uk).

Redundancy has historically been one of the most attractive approaches to provide the failure-tolerant capability to power electronic systems [5]. While being highly effective in this regard, redundant design will normally significantly increase the cost and size of the system, thus compromising its competitiveness in the market. Another scheme is to select the individual components in the converter (e.g. switching devices, inductors, capacitors) with sufficient thermal and electrical stress margin, thus expecting their low failure rates and, consequently, high reliability of the overall system. However, with this approach, the quantitative reliability metrics of individual devices are not taken into account, and for this reason it is also not possible to automatically design the system for pre-specified lifetime.

To circumvent the drawbacks of aforementioned methods, the research in reliability of power electronic systems has recently experienced a paradigm shift towards the so called design for reliability (DfR) approach [6], [7]. The key idea here is take the reliability metrics explicitly into account during the design process. Since the most vulnerable part of power converters are semiconductor devices, the most attention in this research area has been dedicated towards studying their failure modes. To this end, it has been observed that the most common failure modes are associated with packaging, i.e. with die-attach solder fatigue and bond wire damage. Both of these modes are caused by junction temperature cycles and the mean junction temperature of the device during operation. Manufacturers of semiconductor devices have also carried out comprehensive temperature cycling tests and discovered functional relationships between the amplitude and mean value of the junction temperature, and the device lifetime consumption (LC) [8].

Therefore, the research focus in the DfR area has mostly been on investigating the thermal loading of power devices [9]–[11]. These investigations can be carried out either experimentally or using detailed simulations models, which have been shown to match excellently the experimental results [12], [13]. The main principle is to expose the power converter to a mission profile that represents its realistic operating condition and extract the corresponding thermal profile of one or more devices (i.e. the junction temperature data). The mission profile is usually characterized by an ambient temperature and current flowing through the power converter over a certain period of time [14]. The rainflow counting algorithm can then be deployed to count the number of junction temperature swings and to extract their amplitudes as well as mean values from the given thermal profile. Final step is to associate every cycle with its cumulative damage (e.g. using [8] or other device LC

data from the relevant manufacturer), and calculate the overall LC over a period of time using the Miner's rule [9]. Assuming that all other components in the system are significantly more reliable, the LC of power devices is hence normally considered as the representation of the whole system's LC [15]–[18]. It is also possible to combine LCs of several components in the system to assess the system level LC [19].

Nevertheless, the LC estimation procedure in all the DfR approaches mentioned in the existing literature are made on power electronic systems whose design parameters are already fixed. This means that every time a designer would like to check how different design parameters affect the lifetime of power electronic system, he would need to perform the time consuming simulations or experiments all over again. Moreover, with existing methods it is not possible to specify a certain lifetime of the power electronic system as a design goal and then explicitly obtain the design parameters that guarantee the specified LC. In other words, there is no possibility to reverse the design process.

The aim of this paper is to bridge this research gap by building upon the principal DfR concepts and develop a fully automated design for reliability (ADfR) tool. The key enabling methodology for this development is artificial intelligence, and more particularly the artificial neural networks (ANNs). It is well known that ANNs are universal function approximators, i.e. they can approximate any given input/output data relationship with arbitrary precision [20]. Here, we take advantage of this capability for two different purposes. First, we use it to build a surrogate model of the power converter that is able to estimate the thermal stress of any device in the converter as a function of design parameters and the mission profile several orders of magnitude faster compared to running the detailed simulation model. Such a surrogate model, labeled as ANN_1, has similar functionality as a lookup table reported in e.g. [18], but consumes significantly lower amount of memory, thus allowing to embed any design parameter as an input to the model. In addition, it has much better capability to generalize nonlinear input/output data relationship, thereby providing more precise estimates of the junction temperatures. The second purpose of ANN is to establish the functional relationship between design parameters and yearly LC in a network labeled ANN_2. Again, this process resembles the ones presented in [16]–[18], but here the LC evaluation is systematically repeated for a large number of design parameter variations to generate the training data for ANN_2 which, after training, gives an explicit functional relationship between design parameters and LC, thus providing a key basis for ADfR. ANN_2 can consequently be used either individually or in conjunction with other design tools, e.g. if it is desirable to balance the reliability of the system with other metrics such as cost, weight/volume, or others.

The rest of the paper is organized as follows. Section II describes the power electronic system under consideration, i.e. the single-phase grid-connected H-bridge PV inverter, although the proposed methodology is generic and thus applicable to any other converter topology. In Section III, the conventional system design and reliability evaluation methodologies are briefly revised, while Section IV provides the background about the artificial neural networks. In Section V, the proposed design procedure is described step by step. The procedure is then verified in Section VI, where switching frequency and dc-link voltage reference of the grid connected PV inverter that provide the optimal balance between the reliability and size of the system, are found via proposed approach. Finally, the conclusion of the paper is given in Section VII.

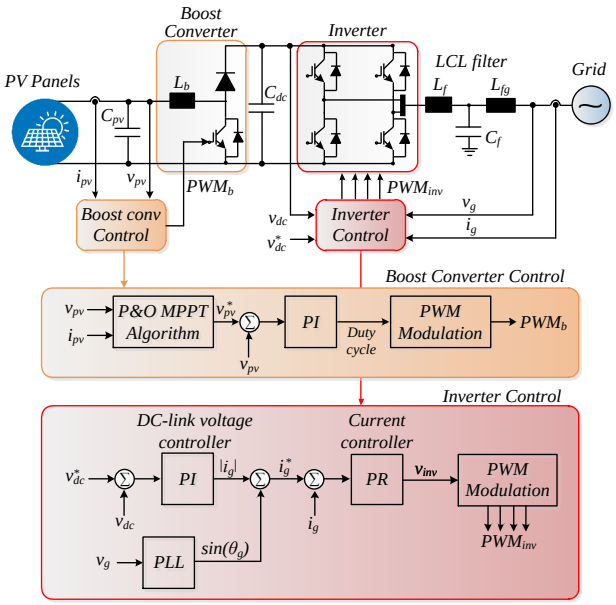

Fig. 1. System configuration and control structure of a two-stage single phase grid-connected PV system. Here, PI is proportional-integral, PR is proportional-resonant, PLL is phase locked loop, PWM is pulse width modulator.

II. Description of the Case Study

A. System Description

The design methodology proposed in this paper is verified on a power electronic system case study that involves a two-stage grid connected single-phase PV inverter with rated power of 10 kW, as shown in Fig. 1. The system comprises a dc-dc boost converter, which operates the maximum power point tracking (MPPT) algorithm and a full-bridge dc-ac converter that regulates the intermediate dc link voltage v_{dc} and grid side current using cascaded linear control loops. The correct angle for the current controller is provided by a phase-locked loop (PLL).

Table I indicates the design parameters of the system. These parameters have a strong influence on its performance, size/cost and reliability, and should therefore be carefully selected. In a case study analyzed in this paper, some of the listed parameters are considered to be fixed while others are designable. For instance, the switching frequency of the inverter f_{sw}, reference dc link voltage v^*_{dc}, and LCL filter parameters (L_f, C_f, L_{fg}) are chosen as designable parameters. By looking at the relationships between these parameters, it is intuitively clear that higher f_{sw} will yield a lower switching ripple, thus permitting the usage of a smaller filter. However, higher switching frequency will also result in higher switching

TABLE I
PARAMETERS OF THE TWO-STAGE SINGLE PHASE PV SYSTEM (FIG. 1)

Fixed parameters	
PV inverter rated power	10 kW
Boost converter inductor	L_b = 1.8 mH
PV-side capacitor	C_{pv} = 1000 μF
Dc-link capacitor	C_{dc} = 1100 μF
Grid nominal frequency	$\omega_g = 2\pi \times 50 rad/s$
Grid nominal voltage (RMS)	230 V
Designable parameters	
Inverter LCL filter	L_f, C_f, L_{fg}
Inverter switching frequency	f_{sw}
Dc-link voltage reference	v_{dc}^*

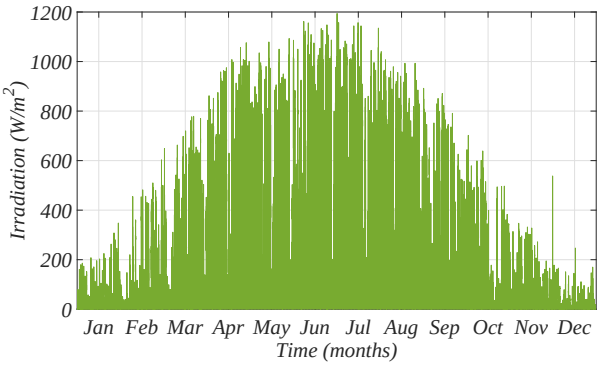

(a) Solar irradiation.

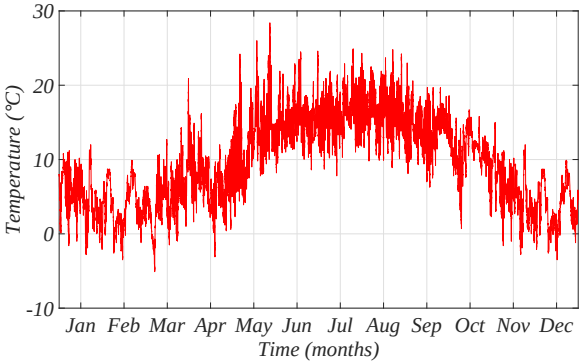

(b) Ambient Temperature.

Fig. 2. Yearly mission profile from the PV installation site in Aalborg, Denmark with a sampling rate of 1 min/sample.

losses, thereby causing larger junction temperatures of the power devices and shortening their lifetime.

While the aforementioned design trade-off between the reliability and size of the system is well-known, the existing research works fail to establish explicit relationships between these two metrics and to embed them as a part of the design process. More particularly, the works labeled under the *Design for Reliability* alias (e.g. [17], [18]) assume predetermined design and only provide lifetime prediction for a given design and mission profile. Therefore, it would be more appropriate to label the methods proposed in these works as reliability evaluation methods. On the other hand, the works that consider optimal design of power electronic systems (e.g. [21]–[24]) do not take into account the reliability of the system as a performance metric. The aim in this paper is to fill this knowledge gap by providing a holistic design methodology that simultaneously takes into account the performance, reliability and size/cost of the system.

B. Mission Profile

Besides the design parameters, the mission profile in which the power converter is operated has a notable impact on the junction temperatures of power devices. Mission profile characterizes the operating conditions such as the ambient temperature and the power processed by the converter. As shown in [18], mission profiles can vary significantly according to geographic location.

In this paper, a yearly mission profile recorded in Aalborg, Denmark has been used for the considered case study, as shown in Fig. 2. It can be seen from the figure that the profile involves yearly irradiation and ambient temperature data. Depending on the particular PV panel characteristics, which can be found in the manufacturer data-sheet, such data can easily be translated into the power processed by the inverter P_{in}, assuming that the maximum possible power is always extracted. P_{in} and T_a can then be used for obtaining the junction temperatures from the detailed simulation model, as detailed in Section III-B.

III. RELIABILITY OF THE POWER ELECTRONIC SYSTEM

In principle, the reliability of power electronic system can be improved in the following three ways [6]: 1) by selecting a suitable topology of the converter, i.e. the one that either minimizes the number of components or that provides redundancy in case of failures 2) by choosing high quality individual components in the system that are less likely to fail, and 3) by reducing the stress level of the components [6].

A. Design Trade-Off

In this paper, it is assumed that the circuit topology of the converter is fixed and that the type of components most prone to failures, i.e. the switching devices, are preselected. To this end, the main design goal from a reliability point of view is to minimize the stress level on the switching devices. As mentioned before, lower f_{sw} leads to lower switching loss, which in turn induces lower temperature swings and hence leads to longer lifetime for the devices. However, lower f_{sw} also results in higher harmonic distortion and in a slower dynamic response of the converter, while it also requires bulkier and more expensive passive filters. Similarly, higher v_{dc} increases the switching losses and causes higher switching ripple [22], but the higher it is, the more control bandwidth it provides [25]. In this respect, it is clear that f_{sw} and v_{dc} are two key design parameters that affect the reliability, performance and size (cost) of the system. Therefore, these two parameters should be explicitly selected to yield the best balance between these metrics.

TABLE II
PARAMETERS OF THE LIFETIME MODEL OF AN IGBT MODULE

A	3.4368×10^{14}
α	-4.923
β_0	1.942
β_1	$-9.012x10^{-3}$
C	1.434
γ	-1.208
f_d	0.6204
ar	0.28
E_a	0.06606 eV
k_b	$8.6173324 \times 10^{-5} eV/K$

In order to provide a framework for truly optimal design, the well-known conventional design procedure (as in e.g. [21] and [22]) is here combined with the LC of the system, which can be considered as its reliability metric. The methodology for evaluating the LC of power devices is described in the following subsection.

B. Lifetime Evaluation Procedure

It is well known that the power devices are the most vulnerable components of power electronic converters. Depending on the mission profile (T_a and P_{in}) and design parameters (v_{dc}, f_{sw}, heat sink parameters and others), these devices will experience junction temperature swings that cause their wear-out. The temperature swings occur due to changing switching and conduction losses caused both by the varying loading (mission profile) and the sinusoidal shape of the inverter current. For a given operating condition, the thermal stress on the device can be characterized by the mean temperature value T_{jm}, the amplitude of oscillation ΔT_j and the period of oscillation t_{on}.

The concrete values of T_{jm}, ΔT_j and t_{on} can be extracted from the detailed simulation model of the converter and its associated thermal network. However, it is unfeasible to run the detailed simulation for the whole yearly mission profile period. For this reason, an approximate model of the converter that can quickly translate the mission profile and design parameters into junction temperatures, is commonly developed. The development of such model using artificial intelligence methodology is described in the following section.

For numerous types of devices, empirical models that quantify the effect of each cycle on the lifetime of the device have been constructed based on experimental data. An example of one such model is given in [8]:

$$N_f = A \times (\Delta T_j)^{\alpha} \times (ar)^{\beta_1 \Delta T_j + \beta_0} \times \left[\frac{C + (t_{on})^{\gamma}}{C+1}\right] \times exp\left(\frac{E_a}{k_b \times T_{jm}}\right) \times f_d, \quad (1)$$

where N_f is the number of cycles that a device can tolerate before failure if stressed with a certain ΔT_j, T_{jm} and t_{on}. The other parameters required to evaluate (1) can be obtained experimentally. An exemplary set of parameters is taken from [8] and it is shown in Table II.

The inverse of N_f indicates the level of damage that a device sustains under certain stress conditions. In line with this, the total LC over a certain period can then be estimated using the Miner's rule as follows:

$$LC = \sum \frac{n_i}{N_{fi}} \quad (2)$$

where n_i is the number of cycles that result in incremental damage $1/N_{fi}$. Therefore, in order to find out the total LC that occurs over a certain time period, it is necessary to count the total number of temperature cycles and associate each cycle with a corresponding N_{fi}.

For a grid-connected PV system, two basic types of junction temperature cycles can be identified. The first type of cycles is caused by the mission profile and they are normally extracted from the yearly junction temperature data using the rain-flow counting algorithm. Such an algorithm extracts all the cycles and associates each one of them with a specific ΔT_j, T_{jm} and t_{on}, thus enabling the usage of (1). The second type is a repercussion of injecting the sinusoidal current at fundamental frequency into the grid. Therefore, this type has a fixed period t_{on}, while given ΔT_j and T_{jm} can be extracted from the converter model and the rain-flow counting data, respectively. Therefore, the total LC can be calculated by adding the two contributions. It should also be noted that the parameters in (1) are usually not deterministic and can vary within certain ranges. If these effects are taken into account, the overall LC is normally evaluated using the Monte-Carlo analysis and represented as the probability distribution function [26]. However, the consideration of the parameter variations in (1) is out of the scope of this paper, and will be considered in the future work.

IV. ANN BASED MODELING

A. Motivation for Using the ANNs

As explained in the previous section, it is essential to establish a simple model of the converter that would be able to translate the yearly mission profile data into a yearly junction temperature variation. The state of the art approaches deal with this task by simulating the detailed model of the converter with associated thermal network for several selected combinations of P_{in} and T_a and extracting the corresponding ΔT_j and T_{jm}. These data are then fed to the look-up table (LUT) that serves as a surrogate model of the converter.

However, there are several fundamental limitations associated with this approach. First, LUTs are not suitable for high-dimensional data mapping since they suffer from the inefficient use of memory space. This is particularly restricting if one would seek to construct a more complicated surrogate model of the power electronic system where it would be required to map both the mission profile and design parameters to the junction temperatures. Secondly, LUTs are unable to learn general nonlinear relationships between the input data and output data since they are based on linear interpolation. While the second issue could be improved by using more data points, this would not be feasible in high-dimensional spaces due to limited memory. For these reasons, LUTs have been only used to map mission profile data (i.e. P_{in} and T_a) to junction

temperatures, assuming that all other design parameters are fixed [18].

In order to come around this difficulty, in this paper we propose the usage of a forward artificial neural network (ANN) to serve as a more fast, accurate and flexible surrogate model of the converter. It has been shown in [20] that forward ANN is a universal function approximator, i.e. that the parameters in its structure can be adjusted in such a way to approximate any nonlinear input/output data relationship with arbitrary precision. For this reason, ANN has better generalization capability than LUT and can thus better approximate the responses to input samples that are outside the training data set. Another advantage of ANN is that the number of training parameters (i.e. weights and bias terms) can generally be several orders of magnitude lower than the number of data points. For this reason, ANN has much lower memory requirements than LUT. In particular, the evaluation of the ANN used in this paper was found to be around four orders of magnitudes faster than the LUT. Finally, ANN is based on a nonparametric regression model. In this case, designer does not need to know anything about the relationship between input and output data, because the ANN will learn them automatically during the training process. This is particularly useful in multi-dimensional spaces where parametric nonlinear regression approaches are not suitable since it is difficult to guess the structure of the function that best models input-output data relationships.

The following subsection provides a brief theoretical introduction to ANNs.

B. ANN Principle

Numerous types of ANNs have been proposed in the literature [27]. Particular network choice depends mostly on the nature of relationships between inputs and outputs in the data. When outputs depend on historical values of the inputs and outputs, recurrent neural networks are the most suitable. In the case study of this paper, the relationship between design parameters and mission profiles with the junction temperatures is static. For this reason, forward ANN has been selected for the case-study here. Forward ANNs are the most commonly used deep learning algorithms and have been applied already to various electrical engineering problems, from predicting the voltage voltage distortion in electrical distribution networks [28], to designing the microwave filters [29], [30].

A forward ANN comprises an input layer, one or more hidden layers, and an output layer. Each of these layers comprises a number of neurons that process the information coming from neurons in the layer below. To calculate the output of a certain neuron γ_i^l in layer l, the outputs of all the neurons z_j^{l-1} ($j = [1..N_{l-1}]$) in the layer below $l-1$ are multiplied with given weights ω_{ij}^l and the bias term b_i^l is then added. The result is processed through an activation function σ that usually takes the form of a sigmoid function, i.e. $\sigma(\gamma) = 1/(1+e^{-\gamma})$, to generate the output z_i^l. This output then becomes one of the inputs for the layer above, $l+1$, and the same procedure is repeated to calculate the output of other neurons in layer l.

In the input layer, z_i^1 takes the form of inputs. On the other hand, the output layer typically uses the linear activation function to allow any numerical value, as opposed to being limited to [0,1] range as the sigmoid function. To sum up, the complete signal flow of the ANN can be described as follows:

- Layer 1 (input):

$$z_i^1 = x_i \quad i = 1, .., N_1 \tag{3}$$

  where x_i are the inputs.
- Layers l = 2,..,$L-1$ (hidden):

$$z_i^l = \sigma\left(\sum_{j=1}^{N_{l-1}} w_{ij}^l z_j^{l-1} + b_i^l\right) \quad i = 1, .., N_l. \tag{4}$$

- Layer L (output):

$$y_i = w_i^L z_i^L \quad i = 1, .., N_L \tag{5}$$

  where y_i are the outputs.

It has been shown in [20] that forward ANN is an universal function approximator, i.e. that the weights and bias terms in its structure can be adjusted so as to approximate any input/output data relationships with arbitrary precision. These parameters are adjusted during the training process, normally using the back-propagation algorithm. This algorithm takes advantage of the continuous differentiability of the ANN to find out the direction in which the w_{ij}^l and b_i^l parameters should be adjusted in each training iteration to reduce the error between the measured output data and prediction made by the ANN from previous iterations [31]. Back-propagation is a well known algorithm that is available in standard softwares like Matlab.

It is important to notice that, before starting the training process, the structure of the network should be defined (i.e. the number of layers and the number of neurons in each layer). To this end, if too few neurons are used, the strong nonlinear relationships may not be captured. On the other hand, overfitting may occur in ANNs with too many neurons. However, up until now, an analytic method for selection for proper number of neurons has not been established. Therefore, they are usually selected using trial-and-error and this approach is also used in this paper.

Next subsection presents the development of two ANNs that are used in the proposed optimal design procedure, which is detailed in Section V.

C. Deployment of ANNs for Fast and Flexible LC Evaluation of the PV Inverter

This section elaborates the development of two dedicated ANNs, one that serves as a surrogate model of the converter and one that translates the design parameters into a yearly LC.

1) ANN1: Surrogate Model of the PV Inverter: The purpose of this network is to map the operating conditions and design parameters into the junction temperatures and is labeled as ANN_1. The data required to train this network is collected by running a detailed simulation model of the converter numerous times to cover some specific range of input parameter variations. After each simulation, corresponding $T_{jm,i,data}$ and $\Delta T_{j,i,data}$ are extracted.

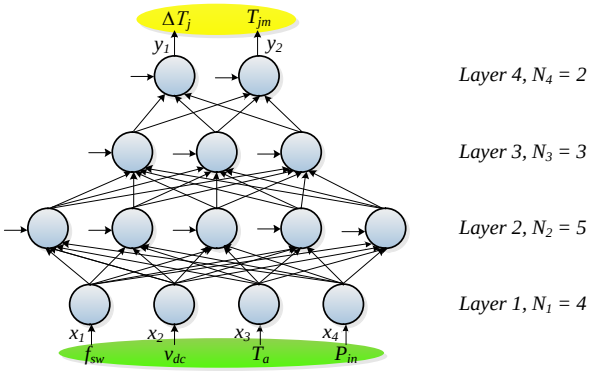

Fig. 3. Structure of the ANN_1. For simplicity, weights and bias terms are omitted from the figure. The inputs to the ANN_1 are highlighted with green color, while the outputs with yellow.

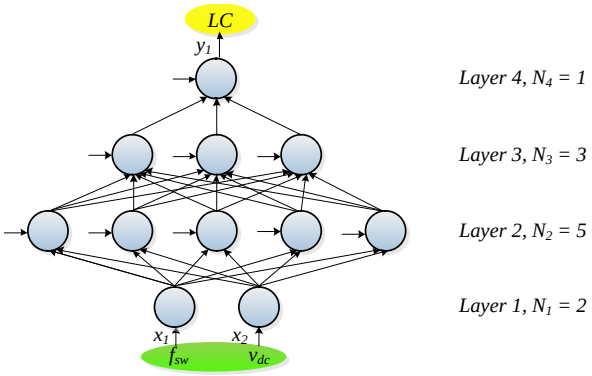

Fig. 4. Structure of the ANN_2. For simplicity, weights and bias terms are omitted from the figure. The inputs to the ANN_2 are highlighted with green color, while the outputs with yellow.

Concerning the structure of the network, it has been empirically chosen to comprise an input layer, two hidden layers, and an output layer, and it is shown in Fig. 3. Therefore, there are 4 layers (L = 4) in total. The number of neurons in the input layer is 4 (N_1 = 4) since there are 2 design parameters v_{dc}^* and f_{sw} and two mission profile parameters, P_{in} and T_a. The number of layers in the two hidden layers are 5 and 3, respectively (N_2 = 5, N_3 = 3). Finally, the output layer comprises 2 neurons (N_4 = 2) because it is of interest to find out two values that characterize the junction temperature, i.e. its mean value T_{jm} and the amplitude of oscillation at fundamental frequency ΔT_j.

After specifying the data sets and structure of the network, ANN_1 was trained using the *train* command, which is a part of Matlab's Deep Learning Toolbox. Trained ANN_1 can now be used to translate the tunable design parameters and the mission profiles given in Fig. 2 into a junction temperature of the inverter's devices for any given combination of design parameters v_{dc}^* and f_{sw}. Next, ANN_1 is put to use in order to create ANN_2, as detailed below.

2) ANN2: Mapping of Design Parameters to Lifetime of the Inverter: Besides ANN_1, another network labeled as ANN_2 is trained. This network serves as the overall representation of the system that maps the LC for a given yearly mission profile and design parameters. The data required to train this network is collected by running the cycle counting and performing the Miner's rule on a yearly junction temperature data (obtained by evaluating ANN_1 on a yearly mission profile data) for numerous combinations of design parameters f_{sw} and v_{dc}^*, as shown in Fig. 5. Therefore, ANN_1 is automatically embedded in ANN_2. Once the network is trained, instead of running the rainflow counting algorithm every time when the LC estimate is needed, the LC can simply be obtained by evaluating ANN_2.

The structure of this particular network is shown in Fig. 4. It was empirically selected to have an input layer, two hidden layers, and an output layer. The number of neurons in the input layer are 2 (N_1 = 2) since there are 2 design parameters v_{dc}^* and f_{sw}. The number of layers in the two hidden layers are 5 and 3, respectively (N_2 = 5, N_3 = 3). Finally, the output layer comprises 1 neuron (N_4 = 1) because our design interest is in 1 performance indicators, i.e. the converter yearly LC for a certain mission profile. After specifying the data sets and structure of the network, ANN_2 was again trained using the *train* command. Trained ANN_2 can now be deployed as a basis for the optimal design and combined with other designed methodologies, as described in the following section that provides the overall framework of the proposed design approach.

V. Proposed Automated Design Approach

The complete workflow of the proposed design approach is shown in Fig. 5. It can be seen that the procedure is split into a training phase that comprises 4 steps and an optimization stage with a single step. The training phase steps have been described in detail in the previous section and are only graphically summarized in Fig. 5. The ultimate result of this phase is trained ANN_2 that serves as the basis for optimal design since it can explicitly map the design parameters to yearly LC.

Nevertheless, minimization of the LC often needs to be balanced with other metrics of the system. In this paper, the idea is to optimize the trade-off between the LC and the system size, while respecting the performance metrics defined by relevant standards. To account for the power electronic system size in quantitative fashion, the standard methodology for the LCL filter design of grid-connected converters is adopted here (e.g. as suggested in [21] and [22]).

Similarly like with lifetime consumption, the required LCL filter parameters are also dependent on the f_{sw} and v_{dc}. The first step is to select the inductance of the converter side inductor L_f, which is normally done in accordance with maximum permissible ripple in the converter current, as follows [22]:

$$L_f = \frac{v_{dc}}{6 f_{sw} \Delta I_{Lmax}}. \tag{6}$$

where ΔI_{Lmax} is usually selected to be 10 % of the rated converter current. The filter capacitor C_f is then selected to limit the reactive power consumption of the filter. Usually, its value is limited to 5 % of the base capacitance value, as follows:

$$C_f \leq 0.05 \cdot \frac{P_n}{\omega_g E_n^2}. \tag{7}$$

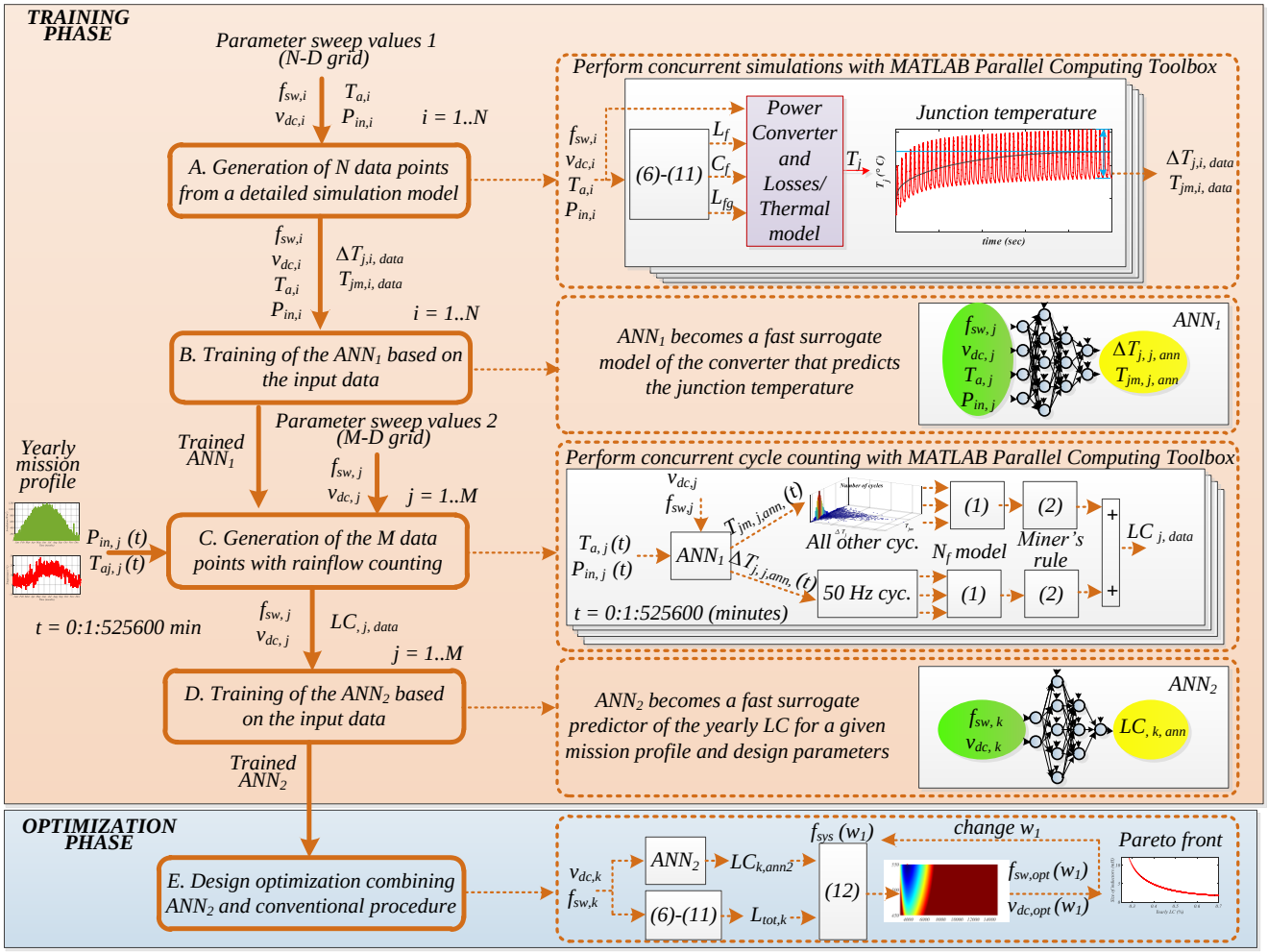

Fig. 5. Flow diagram of the proposed artificial intelligence based design optimization of the power electronic system.

where P_n is the rated power of the converter, ω_g is the grid angular frequency, while E_n is the grid voltage amplitude. The attenuation of the harmonics from the converter side current depends also on the grid side inductor L_{fg}, as follows:

$$\frac{i_g}{i_c} = k_a = \frac{1}{1 + r(1 - L_f C_f \omega_{sw}^2)}. \tag{8}$$

where k_a is a required attenuation.

The equation (8) then provides the basis for the selection of L_{fg}:

$$L_{fg} = \frac{sqrt(1/k_a^2) + 1}{C_f \omega_{sw}}. \tag{9}$$

It can be seen from (9) that the higher the C_f, the lower L_g is needed to achieve the same level of attenuation. Therefore, it is of interest to set the C_f at the upper limit in order to reduce the size of the L_g, which has a more dominant influence on the size of the system. It is also proposed in some references to initially select C_f at a value lower than maximum in order to allow sufficient headroom for iterative re-engineering the design if the resonance frequency of the filter does not meet the following mandatory requirement [21]:

$$10 f_g < f_{res} = \frac{1}{2\pi} \sqrt{\frac{L_f + L_{fg} + L_g}{L_f \left(L_{fg} + L_g\right) C_f}} < 0.5 f_{sw}. \tag{10}$$

Finally, the resonant frequency is taken into account to derive the value for the damping resistor that is connected in series with the capacitor, as follows:

$$R_f = \frac{1}{6\pi f_{ref} C_f}. \tag{11}$$

To sum up, the standard LCL filter design methods take fixed f_{sw} and v_{dc} as inputs and provide the L_f, C_f and L_{fg} as outputs using the set of equations (6)-(10). It should also be noted that (6)-(10) can be used when generating the data for training ANN_1, as indicated in Fig. 5. Considering that there is not much freedom in designing C_f, it is proposed here to use the total size of inductors (L_{tot} = L_f+L_{fg}) alongside with the yearly LC (predicted by ANN_2) to formulate the overall fitness function, as follows:

$$f_{sys}(w_1) = LC_{ann}^2 + w_1 \cdot (L_{tot})^2. \tag{12}$$

where w_1 is the parameter that is used to balance the importance of the two terms. By using different values of w_1, a Pareto front that characterizes the relationships between the reliability and size of the system can be constructed.

The case-study analysis in the next chapter is carried out using the fitness function (12). However, it is important to notice that this particular fitness function is only exemplary and any other one can be easily adopted within the framework of proposed design methodology. For example, detailed calculation of total volume and power losses of the LCL filter has been carried out in [23] using comprehensive models of inductive power components. Consequently, a Pareto front indicating a trade-off between volume and power loss of the filter has been derived. On the other hand, the LCL grid filter of a multimegawatt medium-voltage neutral-point-clamped converter for a wind turbine is designed using the selective harmonic elimination PWM in [24] to improve the converter efficiency. Design considerations concerning filter volume and efficiency could easily be embedded with the design process proposed in this paper by expanding the fitness function (12). Similarly, effect of alternative modulation schemes on converter efficiency could easily be considered by embedding any type of modulator in the simulation model from which the data is extracted. Consequently, the converter power loss could then be embedded in the fitness function (12) as well. Nevertheless, since research on advanced modulation schemes and detailed modeling of inductive components is out of the scope of this paper, these design considerations have not been considered in the case study carried out in the following section.

VI. Case Study

In order to verify the proposed design methodology, a case study for a PV system located in Denmark has been carried out. As already shown in Section II-B, irradiance and temperature data sampled minute by minute was available from a location in Aalborg/Denmark.

A. Data Extraction, Normalization and Training

First and most computationally demanding step in the proposed method is to extract the data required to train ANN_1. A detailed simulation model of the grid connected inverter with associated heat sink and thermal networks was used for this purpose. The model was simulated for 3 sec in order to ensure that the mean junction temperature converges to a steady state value. Such simulation took around 2 minutes in real time.

In this paper, the design and mission profile parameters were swept using 5 values for each parameter except for the dc link voltage where 3 values have been used (since the temperatures have been observed to rise linearly with the increasing dc link voltage). The main reason why this number of data points was enough to represent the power electronic system at hand is a monotonically increasing nature of underlying functional relationships between input and output data. For instance, if the converter processes higher amount of power, T_{jm} and ΔT_j will both be higher. Similarly, higher ambient temperature, higher switching frequency and higher dc link voltage will also cause increased temperatures of devices. Because of the monotonically increasing nature, the strong nonlinearity in these relationships is avoided and it turned out that it is possible to represent accurately the system only with limited number of data points. In this paper, the following parameter sweep values were used:

$$\begin{aligned} P_{in} &= [1000, 3000, 5000, 7000, 10000]\, W; \\ V_{dc} &= [450, 500, 550]\, V; \\ f_{sw} &= [3000, 5000, 7000, 10000, 15000]\, Hz; \\ T_a &= [-10, 0, 15, 25, 35]\, ^\circ C. \end{aligned} \tag{13}$$

Overall number of data points was thus 375 and the same number of simulations needed to be carried out to extract T_{jm} and ΔT_j. All the results were obtained in approximately one hour on a workstation with 24 parallel cores using Matlab's Parallel Computing Toolbox. The overall data set can also be accessed in Matlab (please find *data375.mat* in the Active Content/Multimedia, where variables $Tmean$ and $deltaT$ correspond to the mean temperature and amplitude of temperature swing, respectively).

This data set was then randomly divided into three data sets, i.e. the training set (70 % of data, corresponding to 263 data points), the validation set (15 % of data, corresponding to 56 data points) and the testing set (15 % of data, corresponding to 56 data points). It should be noted that the precision of ANN turned out to be highly robust to data division ratios. Namely, empirical investigation has shown negligible differences in ANN precision if the training set was kept between 15 % and 90 % of overall data. Regular normalization technique was then deployed on the extracted data. To this end, the largest value of each data point was used as its norm and all other values of the same data type were then divided by the norm prior to the training. This procedure prevented the possibility of having different scales of input data, as all data points were in the [0,1] range.

Consequently, ANN_1 was trained and passed the next stage where it was used to generate data for yearly mission profile (see stage C. in Fig. 5). Here the f_{sw} was swept from 3 to 15 kHz with a step of 1 kHz, whereas v_{dc}^* was swept from 450 to 550 V with a step of 10 V. Therefore, the total number of data points was 143. The whole data collection process was executed in less than 25 seconds, again by using Matlab's Parallel Computing Toolbox. As mentioned before, 50 Hz junction temperature cycles were counted automatically while the other cycles were counted using a rainflow counting algorithm. As with ANN_1, this data set was randomly divided into three data sets, i.e. the training set (70 % of data, corresponding to 101 data points), the validation set (15 % of data, corresponding to 21 data points) and the testing set (15 % of data, corresponding to 21 data points). Data was also normalized. Finally, ANN_2 was trained on a given data and passed forward to the optimization phase.

B. Design Optimization

After the training phase was accomplished, trained ANN_2 was used in the optimization stage together with conventional

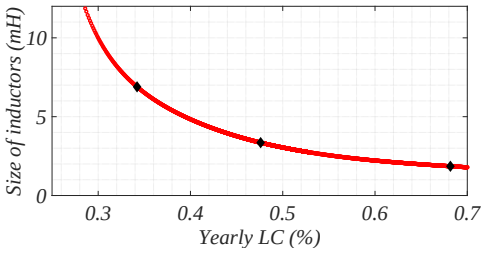

Fig. 6. Pareto front of optimal designs obtained by sweeping the parameter w_1 from (12) from 0 to 25. The three black diamonds correspond to $w_1 = 0.1$, $w_1 = 1$, and $w_1 = 10$, respectively (plots of corresponding fitness functions are shown in Figs. 7-9).

design procedure, as indicated at the bottom of Fig. 5. In particular, the minimum of the fitness function (12) was calculated for different parameter values of w_1, which was swept from 0 to 25. As an example, three arbitrary points corresponding to three different w_1 (for w_1 = 0.1, w_1= 1 and w_1 = 10, respectively) have been selected from a given curve. The super-high-fidelity plots of associated fitness functions (together with optimal design parameters and corresponding total filter inductance, as well as LC) are given in Figs. 7, 8 and 9, respectively. The respective minimums have been found using an exhaustive search algorithm, which is feasible for this case study since the evaluation of ANN_2 is computationally extremely light (around 0.1 μsec). For comparison, a commonly used look-up table that comprises the same dataset turned out to be significantly more computationally intensive as it took approximately 800 μsec to evaluate it. While this time can still be considered relatively short, it would quickly present a limitation when sweeping through the whole design space with high fidelity.

Fig. 6 shows the Pareto front that shows the yearly LC and the filter size corresponding to minimums of many fitness functions obtained by sweeping the parameter w_1 from 0 to 25. The obtained Pareto front clearly illustrates the trade-off between the yearly LC and size of the system and provides the formal framework for optimal design. Considering fast evaluation of the fitness function (12), each of the 4-megapixel plots shown in Fig. 7 and Fig. 8 and Fig. 9 were generated in less than 0.5 seconds. The optimal solution was then simply obtained by finding the lowest value in the given plot, which can be done in Matlab almost instantaneously using the embedded min function.

It also needs to be noted that if more design parameters should be considered, the computational burden of the exhaustive search method might become too high. If this happens, there are several alternative ways to do the minimization. One possibility may be to evaluate fitness function sequentially, with higher and higher fidelity. Another option could be to apply advanced approaches such as evolutionary optimization. This would not impose strict limitation on the number of design parameters, but would bring risk of getting stuck in local minimums.

VII. Conclusions and Future Work

In this paper, an artificial intelligence aided methodology for design optimization of power electronic systems has been

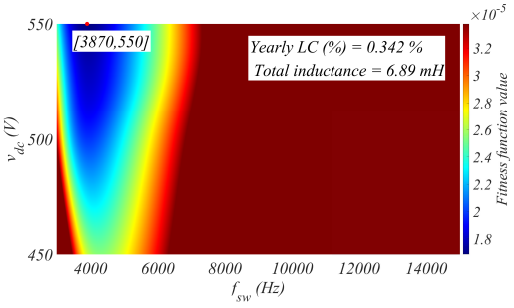

Fig. 7. Plot of the fitness function (12) for $w_1 = 0.1$. The optimum is achieved for f_{sw} = 3870 Hz and v^*_{dc} = 550 V, resulting in yearly LC of 0.342 % and L_{tot} = 6.89 mH.

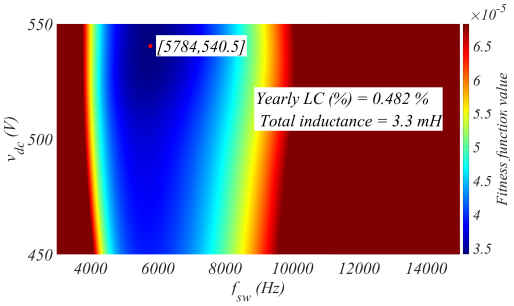

Fig. 8. Plot of the fitness function (12) for $w_1 = 1$. The optimum is achieved for f_{sw} = 5784 Hz and v^*_{dc} = 540.5 V, resulting in yearly LC of 0.482 % and L_{tot} = 3.3 mH.

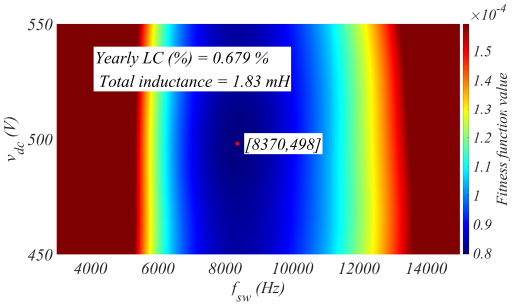

Fig. 9. Plot of the fitness function (12) for $w_1 = 10$. The optimum is achieved for f_{sw} = 8370 Hz and v^*_{dc} = 498 V, resulting in yearly LC of 0.679 % and L_{tot} = 1.83 mH.

proposed. The fundamental idea behind the method is to substitute the key two steps of the system's standard reliability evaluation procedure with dedicated ANNs that serve as fast and accurate approximations of these steps. As shown in Fig. 5, the first one, ANN_1, is trained to act as a surrogate model of the power electronic converter that can map the operating conditions and design parameters into junction temperature(s) of the converter's power devices. The other one, ANN_2, is then trained using both ANN_1 and any given mission profile (e.g yearly) to serve as an overall system representation that maps the design parameters into a LC. Since ANN can be evaluated extremely fast (around 1 μsec), numerous design parameter combinations can be tested almost instantaneously in order to shed light on their influence of design goals. Here, this capability was exploited in order to formally investigate the influence of two exemplary design parameters, i.e. f_{sw}

and v_{dc}^* on the trade-off between the filter size in the single-phase grid-connected PV system and the LC of the devices in the converter. With aid of proposed methodology, this trade-off was represented with the Pareto curve that provides the precise design limitations of the system and allows one to analytically find the optimal f_{sw} and v_{dc}^* in accordance to desired position on the Pareto curve. This provides a clear improvement over the state of the methods that can only evaluate the LC for a fixed design and allows powerful design optimization capability. Possible interesting directions for the future work could be to look at more design parameters (e.g. heat sink parameters, modulation strategy, etc.). This would prolong the data extraction process, but the trained neural network could then be used for more comprehensive design optimization. Another research direction could be to embed more performance metrics such as the volume and cost of the system. Finally, it would be interesting to investigate the proposed system design procedure on types of power electronic converters that exhibit unequal thermal stress distribution among their devices.

ACKNOWLEDGMENT

The authors would like to thank Ariya Sangwongwanich for his help in setting up the simulation model of the power electronic system shown in Fig. 1.

REFERENCES

[1] F. Blaabjerg, Z. Chen, and S. Kjaer, "Power Electronics as Efficient Interface in Dispersed Power Generation Syst.," *IEEE Trans. on Power Electron.*, vol. 19, pp. 1184–1194, Sept. 2004.

[2] T. Dragicevic, X. Lu, J. C. Vasquez, and J. M. Guerrero, "DC Microgrids-Part II: A Review of Power Architectures, Applications, and Standardization Issues," *IEEE Trans. on Power Electron.*, vol. 31, pp. 3528–3549, May 2016.

[3] A. Golnas, "Pv system reliability: An operator's perspective," *IEEE J. of Photovolt.*, vol. 3, pp. 416–421, Jan 2013.

[4] V. N. Ferreira, A. F. Cupertino, H. A. Pereira, A. V. Rocha, S. I. Seleme, and B. Cardoso, "Design and selection of high reliability converters for mission critical industrial applications: A rolling mill case study," *IEEE Trans. on Ind. Appl.*, vol. Early Access, pp. 1–10, 2018.

[5] J. C. Salmon, "Reliable 3-phase pwm boost rectifiers employing a stacked dual boost converter subtopology," *IEEE Trans. on Ind. Appl.*, vol. 32, pp. 542–551, May 1996.

[6] R. Burgos, G. Chen, F. Wang, D. Boroyevich, W. G. Odendaal, and J. D. V. Wyk, "Reliability-oriented design of three-phase power converters for aircraft applications," *IEEE Trans. on Aer. and Electron. Sys.*, vol. 48, pp. 1249–1263, April 2012.

[7] H. Wang, M. Liserre, and F. Blaabjerg, "Toward reliable power electronics: Challenges, design tools, and opportunities," *IEEE Ind. Electron. Mag.*, vol. 7, pp. 17–26, June 2013.

[8] U. Scheuermann, R. Schmidt, and P. Newman, "Power cycling testing with different load pulse durations," in *7th IET Int. Conf. on Power Electron., Machines and Drives (PEMD 2014)*, pp. 1–6, April 2014.

[9] H. Huang and P. A. Mawby, "A lifetime estimation technique for voltage source inverters," *IEEE Trans. on Power Electron.*, vol. 28, pp. 4113–4119, Aug 2013.

[10] A. Anurag, Y. Yang, and F. Blaabjerg, "Thermal performance and reliability analysis of single-phase pv inverters with reactive power injection outside feed-in operating hours," *IEEE Jour. Emerg. Sel. Topics Power Electron.*, vol. 3, pp. 870–880, Dec 2015.

[11] M. Andresen, G. Buticchi, and M. Liserre, "Thermal stress analysis and mppt optimization of photovoltaic systems," *IEEE Trans. on Ind. Electron.*, vol. 63, pp. 4889–4898, Aug 2016.

[12] K. Ma, M. Liserre, F. Blaabjerg, and T. Kerekes, "Thermal loading and lifetime estimation for power device considering mission profiles in wind power converter," *IEEE Trans. on Power Electron.*, vol. 30, pp. 590–602, Feb 2015.

[13] A. S. Bahman, K. Ma, P. Ghimire, F. Iannuzzo, and F. Blaabjerg, "A 3-d-lumped thermal network model for long-term load profiles analysis in high-power igbt modules," *IEEE J. Emerg. Sel. Topics Power Electron.*, vol. 4, pp. 1050–1063, Sept 2016.

[14] S. E. D. Len-Aldaco, H. Calleja, F. Chan, and H. R. Jimnez-Grajales, "Effect of the mission profile on the reliability of a power converter aimed at photovoltaic applicationsa case study," *IEEE Trans. on Power Electron.*, vol. 28, pp. 2998–3007, June 2013.

[15] Y. Song and B. Wang, "Survey on reliability of power electronic systems," *IEEE Trans. on Power Electron.*, vol. 28, pp. 591–604, Jan 2013.

[16] M. Musallam, C. Yin, C. Bailey, and M. Johnson, "Mission profile-based reliability design and real-time life consumption estimation in power electronics," *IEEE Trans. on Power Electron.*, vol. 30, pp. 2601–2613, May 2015.

[17] N. C. Sintamarean, F. Blaabjerg, H. Wang, F. Iannuzzo, and P. de Place Rimmen, "Reliability oriented design tool for the new generation of grid connected pv-inverters," *IEEE Trans. on Power Electron.*, vol. 30, pp. 2635–2644, May 2015.

[18] A. Sangwongwanich, Y. Yang, D. Sera, and F. Blaabjerg, "Lifetime evaluation of grid-connected pv inverters considering panel degradation rates and installation sites," *IEEE Trans. on Power Electron.*, vol. 33, pp. 1225–1236, Feb 2018.

[19] D. Zhou, G. Zhang, and F. Blaabjerg, "Optimal selection of power converter in dfig wind turbine with enhanced system-level reliability," *IEEE Trans. on Ind. Appl.*, vol. Early Access, pp. 1–9, 2018.

[20] K. Hornik, M. Stinchcombe, and H. White, "Multilayer feedforward networks are universal approximators," *Neural Networks*, vol. 2, no. 5, pp. 359 – 366, 1989.

[21] M. Liserre, F. Blaabjerg, and S. Hansen, "Design and control of an lcl-filter-based three-phase active rectifier," *IEEE Trans. on Ind. Appl.*, vol. 41, no. 5, pp. 1281–1291, 2005.

[22] A. Reznik, M. G. Simoes, A. Al-Durra, and S. M. Muyeen, "*lcl* filter design and performance analysis for grid-interconnected systems," *IEEE Trans. on Ind. Appl.*, vol. 50, pp. 1225–1232, March 2014.

[23] J. Muhlethaler, M. Schweizer, R. Blattmann, J. W. Kolar, and A. Ecklebe, "Optimal design of lcl harmonic filters for three-phase pfc rectifiers," *IEEE Trans. on Power Electron.*, vol. 28, pp. 3114–3125, July 2013.

[24] M. Zabaleta, E. Burguete, D. Madariaga, I. Zubimendi, M. Zubiaga, and I. Larrazabal, "Lclgrid filter design of a multimegawatt medium-voltage converter for offshore wind turbine using shepwm modulation," *IEEE Trans on Power Electron*, vol. 31, pp. 1993–2001, March 2016.

[25] D. G. Holmes, T. A. Lipo, B. P. McGrath, and W. Y. Kong, "Optimized design of stationary frame three phase ac current regulators," *IEEE Trans. on Power Electron.*, vol. 24, pp. 2417–2426, Nov 2009.

[26] P. D. Reigosa, H. Wang, Y. Yang, and F. Blaabjerg, "Prediction of bond wire fatigue of igbts in a pv inverter under a long-term operation," *IEEE Trans. on Power Electron.*, vol. 31, pp. 7171–7182, Oct 2016.

[27] J. Schmidhuber, "Deep learning in neural networks: An overview," *Neural Networks*, vol. 61, pp. 85 – 117, 2015.

[28] B. Singh, V. Verma, and J. Solanki, "Neural network-based selective compensation of current quality problems in distribution system," *IEEE Trans. on Ind. Electron.*, vol. 54, pp. 53–60, Feb 2007.

[29] Q.-J. Zhang, K. C. Gupta, and V. K. Devabhaktuni, "Artificial neural networks for rf and microwave design - from theory to practice," *IEEE Trans. Microw. Theory Tech.*, vol. 51, pp. 1339–1350, Apr 2003.

[30] H. Kabir, Y. Wang, M. Yu, and Q. J. Zhang, "Neural network inverse modeling and applications to microwave filter design," *IEEE Trans. Microw. Theory Tech.*, vol. 56, pp. 867–879, April 2008.

[31] D. E. Rumelhart, G. E. Hinton, and R. J. Williams, "Learning representations by back-propagating errors," *Nature*, vol. 323, Oct 1986.

Tomislav Dragičević (S'09-M'13-SM'17) received the M.Sc. and the industrial Ph.D. degrees in Electrical Engineering from the Faculty of Electrical Engineering, Zagreb, Croatia, in 2009 and 2013, respectively. From 2013 until 2016 he has been a Postdoctoral research associate at Aalborg University, Denmark. From March 2016 he is an Associate Professor at Aalborg University, Denmark where he leads an Advanced Control Lab.

He made a guest professor stay at Nottingham University, UK during spring/summer of 2018. His principal field of interest is design and control of microgrids, and application of advanced modeling and control concepts to power electronic systems. He has authored and co-authored more than 155 technical papers (more than 55 of them are published in international journals, mostly IEEE Transactions) in his domain of interest, 8 book chapters and a book in the field.

He serves as a Guest Editor in Chief for IEEE TRANSACTIONS ON ENERGY CONVERSION, Associate Editor in the IEEE TRANSACTIONS ON INDUSTRIAL ELECTRONICS and as Associate Editor in the Journal of Power Electronics. Dr. Dragičević is a recipient of the Končar prize for the best industrial PhD thesis in Croatia, and a Robert Mayer Energy Conservation award.

Patrick Wheeler (M'90-SM'04) received his BEng [Hons] degree in 1990 from the University of Bristol, UK. He received his PhD degree in Electrical Engineering for his work on Matrix Converters from the University of Bristol, UK in 1994.

In 1993 he moved to the University of Nottingham and worked as a research assistant in the Department of Electrical and Electronic Engineering. In 1996 he became a Lecturer in the Power Electronics, Machines and Control Group at the University of Nottingham, UK. Since January 2008 he has been a Full Professor in the same research group. He was Head of the Department of Electrical and Electronic Engineering at the University of Nottingham from 2015 to 2018. He is currently the Head of the Power Electronics, Machines and Control Research Group and is the Li Dak Sum Chair Professor in Electrical and Aerospace Engineering at the University of Nottingham, China. He is a member of the IEEE PELs AdCom and was an IEEE PELs Distinguished Lecturer from 2013 to 2017. He has published 500 academic publications in leading international conferences and journals.

Frede Blaabjerg (S'86-M'88-SM'97-F'03) was with ABB-Scandia, Randers, Denmark, from 1987 to 1988. From 1988 to 1992, he got the PhD degree in Electrical Engineering at Aalborg University in 1995. He became an Assistant Professor in 1992, an Associate Professor in 1996, and a Full Professor of power electronics and drives in 1998. From 2017 he became a Villum Investigator. He is honoris causa at University Politehnica Timisoara (UPT), Romania and Tallinn Technical University (TTU) in Estonia.

His current research interests include power electronics and its applications such as in wind turbines, PV systems, reliability, harmonics and adjustable speed drives. He has published more than 600 journal papers in the fields of power electronics and its applications. He is the co-author of four monographs and editor of ten books in power electronics and its applications.

He has received 29 IEEE Prize Paper Awards, the IEEE PELS Distinguished Service Award in 2009, the EPE-PEMC Council Award in 2010, the IEEE William E. Newell Power Electronics Award 2014 and the Villum Kann Rasmussen Research Award 2014. He was the Editor-in-Chief of the IEEE TRANSACTIONS ON POWER ELECTRONICS from 2006 to 2012. He has been Distinguished Lecturer for the IEEE Power Electronics Society from 2005 to 2007 and for the IEEE Industry Applications Society from 2010 to 2011 as well as 2017 to 2018. In 2018 he is President Elect of IEEE Power Electronics Society. He serves as Vice-President of the Danish Academy of Technical Sciences. He is nominated in 2014, 2015, 2016 and 2017 by Thomson Reuters to be between the most 250 cited researchers in Engineering in the world.